Editors' Choice

ORIGINAL PAPER

Nagoya J. Med. Sci. **85**. 758–771, 2023
doi:10.18999/nagjms.85.4.758

Pattern of THK 5351 retention in normal aging involves core regions of resting state networks associated with higher cognitive function

Yusuke Yoshida[1], Takamasa Yokoi[2], Kazuhiro Hara[1], Hirohisa Watanabe[3,4], Hiroshi Yamaguchi[5], Epifanio Bagarinao[3], Michihito Masuda[1], Toshiyasu Kato[1], Aya Ogura[1], Reiko Ohdake[3], Kazuya Kawabata[1], Masahisa Katsuno[1], Katsuhiko Kato[5], Shinji Naganawa[6], Nobuyuki Okamura[7], Kazuhiko Yanai[8] and Gen Sobue[3,9]

[1]*Department of Neurology, Nagoya University Graduate School of Medicine, Nagoya, Japan*
[2]*Department of Neurology, Toyohashi Municipal Hospital, Toyohashi, Japan*
[3]*Brain and Mind Research Center, Nagoya University, Nagoya, Japan*
[4]*Department of Neurology, School of Medicine, Fujita Health University, Toyoake, Japan*
[5]*Department of Radiological and Medical Laboratory Sciences, Nagoya University Graduate School of Medicine, Nagoya, Japan*
[6]*Department of Radiology, Nagoya University Graduate School of Medicine, Nagoya, Japan*
[7]*Division of Pharmacology, Faculty of Medicine, Tohoku Medical and Pharmaceutical University, Sendai, Japan*
[8]*Department of Pharmacology, Tohoku University School of Medicine, Sendai, Japan*
[9]*Aichi Medical University, Nagakute, Japan*

ABSTRACT

We aimed to elucidate the distribution pattern of the positron emission tomography probe [18F]THK 5351, a marker for astrogliosis and tau accumulation, in healthy aging. We also assessed the relationship between THK5351 retention and resting state networks. We enrolled 62 healthy participants in this study. All participants underwent magnetic resonance imaging/positron emission tomography scanning consisting of T1-weighted images, resting state functional magnetic resonance imaging, Pittsburgh Compound-B and THK positron emission tomography. The preprocessed THK images were entered into a scaled subprofile modeling/principal component analysis to extract THK distribution patterns. Using the most significant THK pattern, we generated regions of interest, and performed seed-based functional connectivity analyses. We also evaluated the functional connectivity overlap ratio to identify regions with high between-network connectivity. The most significant THK distributions were observed in the medial prefrontal cortex and bilateral putamen. The seed regions of interest in the medial prefrontal cortex had a functional connectivity map that significantly overlapped with regions of the dorsal default mode network. The seed regions of interest in the putamen showed strong overlap with the basal ganglia and anterior salience networks. The functional connectivity overlap ratio also showed that three peak regions had the characteristics of connector hubs. We have identified an age-related spatial distribution of THK in the medial prefrontal cortex and basal ganglia in normal aging. Interestingly, the distribution's peaks are located in regions of connector hubs that are strongly connected to large-scale resting state networks associated with higher cognitive function.

Keywords: [18F]THK5351, positron emission tomography (PET), magnetic resonance imaging (MRI), monoamine oxidase-B (MAO-B), resting state networks (RSNs)

Received: June 21, 2022; accepted: December 22, 2022

Corresponding Author: Gen Sobue, MD, PhD
Brain and Mind Research Center, Nagoya University, 65 Tsurumai-cho, Showa-ku, Nagoya 466-8550, Japan
E-mail: sobueg@med.nagoya-u.ac.jp

Abbreviations:
AD: Alzheimer's disease
FC: functional connectivity
fMRI: functional magnetic resonance imaging
mPFC: the medial prefrontal cortex
MAO-B: monoamine oxidase-B
MRI: magnetic resonance imaging
PET: positron emission tomography
PiB: Pittsburgh Compound-B
ROI: region of interest
RSNs: resting state networks
SSM/PCA: subprofile modeling/principal component analysis
SUV: standardized uptake values

INTRODUCTION

Recent progress in imaging techniques, such as positron emission tomography (PET) and magnetic resonance imaging (MRI), has enabled the visualization of not only amyloid β and tau deposition, but also astrogliosis and alterations to anatomical and functional brain networks. These imaging techniques have enabled researchers to examine simultaneously the deposition patterns of abnormal proteins, gray matter atrophic changes, and functional alterations in living diseased brain.

[18F]THK 5351 was initially developed as a tau tracer[1] but became recognized mainly as a monoamine oxidase-B (MAO-B) tracer.[2,3] Its retention corresponded well to the known distribution of tau related to astrogliosis and to increased MAO-B associated with the clinical severity and symptomatology of cognitive decline.[1,3,4] Head-to-head comparison study demonstrated that THK5351 was superior to C-L-deprenyl for visualizing lesions undergoing astrogliosis.[5]

Resting-state functional MRI (fMRI) has also proven to be very useful in examining the brain connectome of both healthy subjects and patients. Alterations in the brain connectome have been associated with psychiatric[6,7] and neurodegenerative disorders.[8-14] In the case of Alzheimer's disease (AD), associations with pathologic proteins and brain network changes have been extensively investigated.[15,16]

Subprofile modeling/principal component analysis (SSM/PCA) is an unbiased data-driven multivariate PCA-based approach. It enables us to identify major sources of variation in the brain image data of both patients and control groups, to reduce the complexity of multivariate data.[17-19]

Using SSM/PCA, we identified a disease-specific spatial pattern of THK 5351 retention composed mainly of three clusters, the precuneus/posterior cingulate cortex, and the right and left dorsolateral prefrontal cortex.[13] Disruption of the functional connections of the precuneus/posterior cingulate cortex, which showed one of the highest retention rates of THK 5351, may play an essential role in the development of dementia.

Only a limited number of imaging studies have explicitly investigated the association between abnormal THK 5351 deposition, volumetric changes, and functional alterations in aging. Recently, Shigemoto et al reported a significant negative correlation between THK 5351 accumulation and gray matter volume in the bilateral medial temporal lobes.[20] However, the spatial pattern of THK 5351 retention in healthy older adults has not been clearly elucidated. Besides, the relationship between THK 5351 retention and resting state networks (RSNs) as assessed by MRI in healthy subjects remains poorly understood.

We aim to identify the patterns which exhibit significant variance in THK 5351 concentration, using SSM/PCA for healthy older adults without amyloid β accumulation or morphological abnormalities. We also investigate the relationship between THK 5351 retention and large-scale RSNs.

PARTICIPANTS AND METHODS

Participants

We enrolled 68 cognitively normal healthy participants in this study. All participants were recruited from the continuing healthy aging cohort study undertaken by the Brain and Mind Research Center of Nagoya University. They underwent MRI/PET scanning at Nagoya University, consisting of T1-weighted anatomical images, Pittsburgh Compound-B (PiB) PET, THK PET, and resting state fMRI data. They underwent cognitive functional testing, which included the mini mental state examination, the Addenbrooke's Cognitive Examination Revised,[21] Alzheimer's Disease Assessment Scale-Cognitive-Japanese, Logical Memory II of the Wechsler Memory Scale Revised, Clinical Dementia Rating, and Clinical Dementia Rating Scale Sum of Boxes. The participants had no history of neurologic or psychiatric illness, no abnormalities upon neurologic examination, no subjective memory complaints, a Clinical Dementia Rating score of zero, an mini mental state examination score of 26 or higher, an Addenbrooke's Cognitive Examination Revised score of 89 or higher, and a score higher than minus one standard deviation of the average of their ages in the Logical Memory II of the Wechsler Memory Scale Revised. No focal deep white matter abnormalities characterized by hyperintensities more severe than grade 2 of the Fazekas hyperintensity rating system were observed in T2-weighted MR images.[22]

This study conformed to the Ethical Guidelines for Medical and Health Research Involving Human Subjects endorsed by the Japanese government and received approval from the Ethics Review Committee of Nagoya University School of Medicine. All participants provided their informed written consent to participate in this study and were treated in accordance with the Declaration of Helsinki.

MRI study

All MRI scans were performed using a Siemens Magnetom Verio (Siemens, Erlangen, Germany) 3.0 T scanner with a 32-channel head coil, at Nagoya University's Brain and Mind Research Center. High-resolution T1-weighted (repetition time = 2.5 s, echo time = 2.48 ms, 192 sagittal slices of 1 mm thickness, field of view = 256 mm, 256 × 256 matrix size) were acquired for anatomical reference. Resting state fMRI scans (8 min, eyes closed) were also acquired (repetition time = 2.5 s, echo time = 30 ms, 39 transverse slices with a 0.5 mm inter-slice interval and 3 mm thickness, field of view = 192 mm, 64 × 64 matrix size, flip angle = 80 degrees). All images were preprocessed using SPM12. The T1-weighted images were first segmented, and the gray matter and white matter components were then used to generate a group template, which was then normalized to Montreal Neurological Institute space, using diffeomorphic anatomical registration using exponentiated lie algebra.

PET study

THK 5351 and PiB were prepared at the Cyclotron and Radioisotope department of Nagoya University. The radiosynthesis of quinoline derivative THK 5351 was prepared from the tosylate precursor (S)-2-(2-methylaminopyrid-5-yl)-6-[[2-(tetrahydro-2H-pyran-2-yloxy)-3-tosyloxy] propoxy] quinoline (THK 5352) according to the previously described method for synthesizing using MPS-200 (Sumitomo Heavy Industries, Japan)[1]. Injectable solutions of THK 5351 were

prepared with a radiochemical purity of more than 95% and a specific activity of 113 ± 50 GBq/μmol. The benzothiazole derivative PiB was radiosynthesized using the one-step 11C-methyl triflate approach from the [N-methyl-11C]-6-OH-BTA-1 precursor (6-OH-BTA-0).[23] PET imaging was performed using a Biograph 16 (Siemens Healthcare, Erlangen, Germany). After injecting 185 MBq of THK 5351 or 555 MBq of PiB, THK 5351 PET images from 50 to 60 min post-injection and PiB PET images from 50 to 70 min post-injection were used for the following analyses.

Regional quantification of PiB PET imaging

We used an automatic program, PMOD's (version 3.7; PMOD Technologies Ltd, Zurich, Switzerland) PNEURO, with brain volumes of interest, automatically using the most likely localization of brain areas as encoded in the maximum probability atlas (N30R83) constructed by Hammers et al.[24] The atlas was adjusted to the individual patient's anatomy with a spatial normalization procedure, which was obtained from the T1-weighted MR image. Standardized uptake values (SUV) images were acquired by normalizing the tissue radioactivity concentration of PiB by injected dose and body weights. The regional SUV of all volumes of interest was divided by the average of both sides of the cerebellar SUV to obtain the SUV ratio of each volume of interest. For PiB PET, if the average SUV ratios of all neocortical areas were less than 1.5, except for the medial temporal lobe, occipital lobe, and pre- and post-central gyrus (global cortical SUV ratio), we assessed the patients as "amyloid β negative."[25-28]

PET (THK 5351) data preprocessing and the spatial distribution pattern analysis

PET (THK 5351) datasets were preprocessed using SPM 12. First, individual images were co-registered to the participants' anatomical images. Using the deformation fields obtained in the segmentation stage, co-registered images were then normalized to the Montreal Neurological Institute space. After normalization, the images were resampled to a $2 \times 2 \times 2$ mm^3 voxel size and smoothed using an 8 mm full width half maximum isotropic 3D Gaussian filter. The preprocessed images were used in the subsequent analyses.

We performed a scaled SSM/PCA on the obtained PET images to identify patterns that exhibited significant variance in THK 5351 concentration. SSM/PCA is a multivariate PCA-based algorithm that identifies major sources of variation in brain image data of both patients and control groups, reducing the complexity of multivariate data. To do this, the preprocessed PET images from all participants were transformed into a two-dimensional matrix where rows represent subjects and columns represent voxels. After applying a logarithmic transform to all elements in the matrix, the mean of each row (subject mean) was computed and subtracted from each row element. After this, the mean value of each column was removed. Finally, the resulting matrix was analyzed using PCA to generate eigenimages and the associated subject-specific eigenimage scores, which represented the similarity of each individual's preprocessed THK 5351 concentration to the SSM/PCA-identified pattern. To delineate a specific AD-related topography, we limited the analysis to the set of principal components that in aggregate accounted for the top 50% of subject × voxel variability, and for which each individual principal component contributed at least 10% to the total variance in the scan data.[29] In the following analysis, we computed the correlation between component subject scores and age.

Resting state fMRI data preprocessing

The resting state fMRI data were also preprocessed using SPM 12. For each participant's data, the first five volumes were removed to account for initial image inhomogeneity. The remaining images were then slice-time corrected, realigned relative to the mean functional image, co-registered to the participant's anatomical image, normalized to the standard Montreal Neurological

Institute space using the deformation fields obtained in the segmentation state, resampled to a $2 \times 2 \times 2$ mm^3 voxel size, and finally, smoothed using an 8 mm full width half maximum 3D Gaussian filter. We further regressed out 24 motion-related signals given by [R_t, R_t^2, R_{t-1}, R_{t-1}^2], where R_t represents the six estimated motion parameters (three for translation and three for rotation) at time *t*, to minimize the effects of head motion. Mean signals from selected regions of interest (ROIs) within white matter and cerebrospinal fluid, the global signal, and derivatives of these signals were also removed, to account for other physiological noise. Finally, the processed images were bandpass filtered within a frequency range from 0.01 Hz to 0.1 Hz. This additional preprocessing of images was performed using in-house Matlab scripts.

Seed-based functional connectivity analysis

To perform seed-based functional connectivity analysis (SBA), using the most significant THK pattern (component 1), we extracted the distribution's peak locations and generated ROIs at those locations. Time series obtained from fMRI within each ROI were extracted, and the mean was computed. To obtain the connectivity between a given ROI and the whole brain, the correlation was estimated between the resulting mean time series and the time series from all voxels within the brain. The correlation values were then converted into z-scores, using Fisher's transform. A one-sample t-test was then performed, including age and sex as covariates of no interest. Significant connectivity values were identified by thresholding the resulting statistical map, using a cluster-level family-wise error corrected to $p < 0.05$, with the cluster-forming threshold set to $p = 0.001$. Finally, we examined the overlap ratio between seed-based functional connectivity (FC) maps and some well-established canonical RSNs. The 90 fMRI atlas (https://findlab.stanford.edu/functional_ROIs.html) was used, consisting of 14 RSNs (dorsal default mode, ventral default mode, precuneus, left and right executive control, anterior and posterior salience, language, visuospatial, basal ganglia, higher and primary visual, and auditory and sensorimotor networks).[30] The functional connectivity overlap ratio (FCOR) was calculated using the following formula[31]:

$$FCOR = \frac{number\ of\ overlapping\ voxels\ between\ FC\ map\ and\ RSN\ template}{number\ of\ cortical\ voxels\ in\ RSN\ template}$$

RESULTS

Clinical characteristics (Table 1)

We excluded six of the 68 initial participants as they showed significant amyloid β accumulation. Cognitive profiles are shown in Table 1. Age showed correlations with Logical Memory II ($r = -0.316$, $p = 0.012$) and Alzheimer's Disease Assessment Scale-Cognitive-Japanese ($r = 0.332$, $p = 0.003$).

There were no significant differences by sex.

Table 1 Clinical characteristics

	Mean(SD)
Age	66.6 (8.8)
Male : Female	23 : 39
MMSE	29.4 (1.2)
ACE-R	97.7 (2.4)
attention	17.8 (0.5)
memory	25.0 (1.4)
fluency	13.7 (1.0)
language	25.5 (0.7)
visuospatial	15.8 (0.6)
Education	14.0 (2.5)
Logical memory II	19.8 (5.9)
ADAS-cog-j	3.3 (1.7)
CDR	0 (0)

MMSE: Mini Mental State Examination
ACE-R: Addenbrooke's Cognitive Examination Revised
ADAS-cog-j: Alzheimer's Disease Assessment Scale-Cognitive-Japanese
CDR: Clinical Dementia Rating

THK 5351 distribution pattern associated with aging

Figure 1 shows the most significant THK distribution pattern (component 1) from SSM/PCA analysis. The pattern mainly included the bilateral medial temporal lobe, hippocampus, putamen, caudate, thalamus, medial prefrontal lobe, anterior cingulate cortex, and orbitofrontal cortex. Correlation analysis showed a significant positive correlation ($r = 0.47$, $p = 0.0001$) between the component score of this pattern and age. Three significant peak locations were identified in the medial prefrontal cortex (mPFC) and bilateral putamen.

Relationship between THK 5351 retention and RSNs from mPFC

The results of the SBA showed that the seed ROI in the mPFC was positively correlated to the medial frontal cortex, posterior cingulate cortex, precuneus, hippocampus, and inferior temporal lobule. These regions overlapped with the default mode network. Conversely, the seed ROI in the mPFC was negatively correlated to the surrounding intraparietal sulcus and occipital lobe. These regions overlapped with the dorsal attention network (Figure 2).

A FCOR analysis showed that positively correlated regions from the ROI in the mPFC had more than 90% overlap with the dorsal default mode network (Figure 4). Five additional RSNs (left executive control, language, basal ganglia, anterior salience, and the precuneus networks) also significantly overlapped with the mPFC ROIs FC map, with FCOR values greater than 20%. Conversely, negatively correlated regions showed more than 80% overlap with the visuospatial network, more than 60% with the primary and high visual networks, and more than 30% with the posterior salience network.

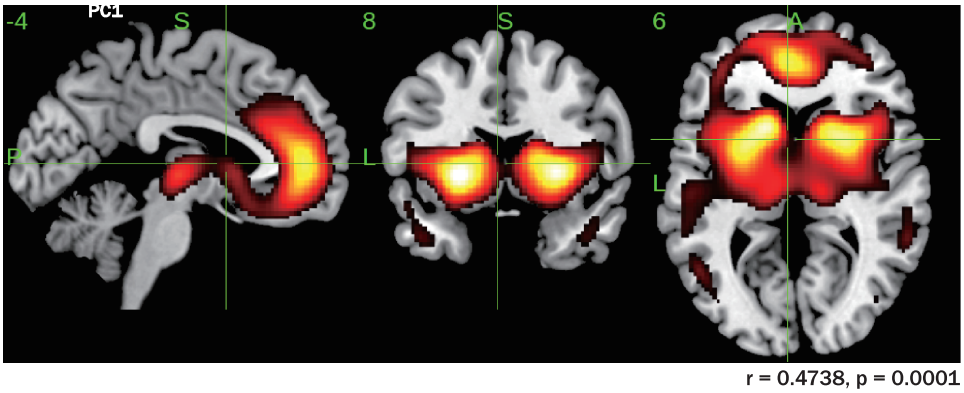

Fig. 1 THK distribution pattern from SSM/PCA
The pattern mainly includes the bilateral medial temporal lobe, hippocampus, putamen, caudate, thalamus, medial prefrontal lobe, anterior cingulate cortex, and orbitofrontal cortex. Correlation analysis showed a significant positive correlation (r = 0.47, p = 0.0001) between the component score of this pattern and age.
SSM/PCA: subprofile modeling/principal component analysis

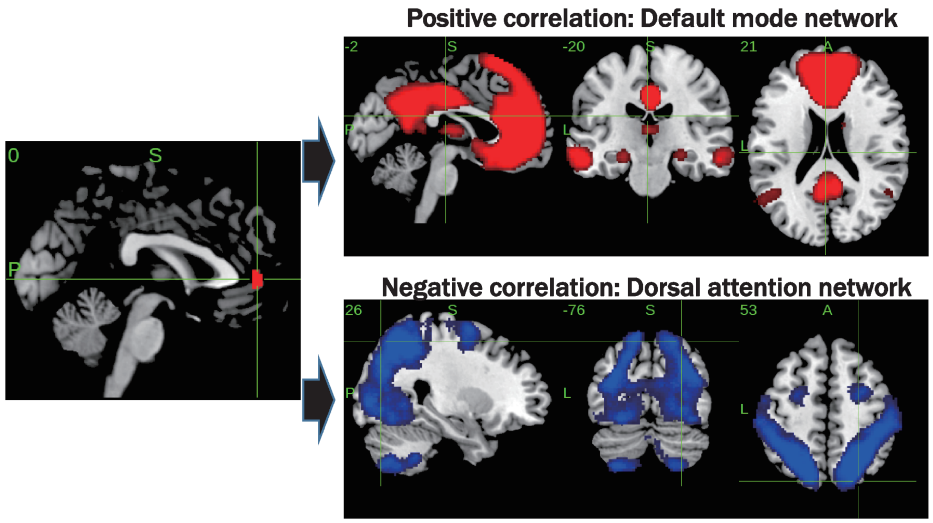

Fig. 2 Relationship between THK 5351 retention and RSNs from mPFC
The results of the SBA showed that the seed ROI in the mPFC was positively correlated to the medial frontal cortex, posterior cingulate cortex, precuneus, hippocampus, and inferior temporal lobule, but negatively correlated to the surrounding intraparietal sulcus and occipital lobe.
mPFC: the medial prefrontal cortex
ROI: region of interest
RSNs: resting state networks
SBA: seed based functional connectivity analysis

Relationship between THK 5351 retention and RSNs from putamen

The results of the SBA showed that the seed ROI in the putamen was positively correlated to the basal ganglia, insula, and dorsal anterior cingulate cortex. These regions overlapped with the basal ganglia/salience networks. However, the seed ROI in the putamen was negatively correlated to the intraparietal sulcus and occipital lobe. These regions overlapped with the dorsal attention network (Figure 3).

Seed ROIs in the putamen had FC maps that overlapped with more than 90% of the basal ganglia network and more than 60% of the anterior salience network (Figure 4). Significant but limited overlap regions also existed with the auditory, sensorimotor, and dorsal default mode networks. Negative FC maps overlapped with more than 90% of the primary visual network. Significant but limited overlap regions also existed in the ventral default mode, high visual, sensorimotor, precuneus, visuospatial and dorsal default mode networks.

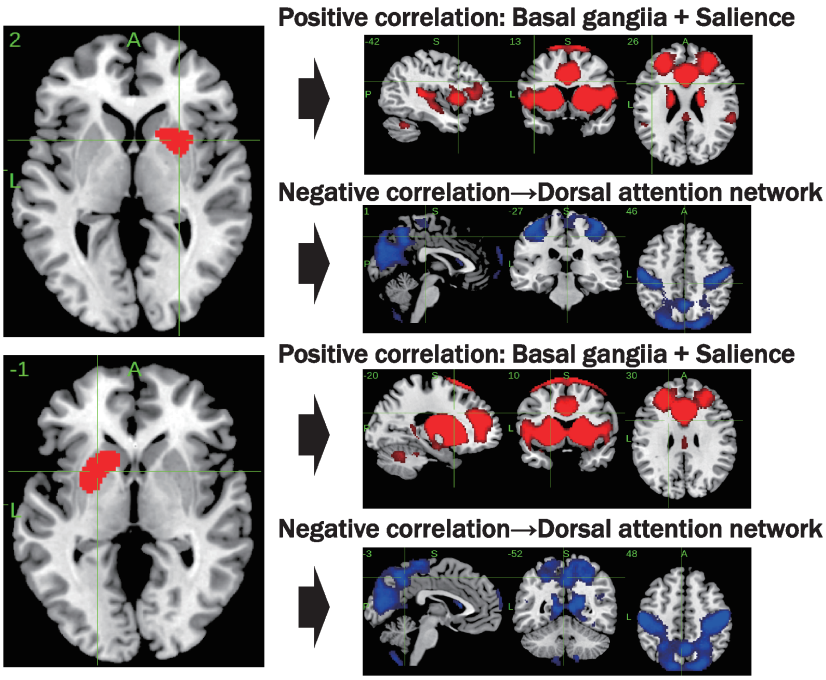

Fig. 3 Relationship between THK 5351 retention and RSNs from putamen
The results of the SBA showed that the seed ROI in the putamen was positively correlated to the basal ganglia, insula, and dorsal anterior cingulate cortex, but negatively correlated to the intraparietal sulcus and occipital lobe.
ROI: region of interest
RSNs: resting state networks
SBA: seed based functional connectivity analysis

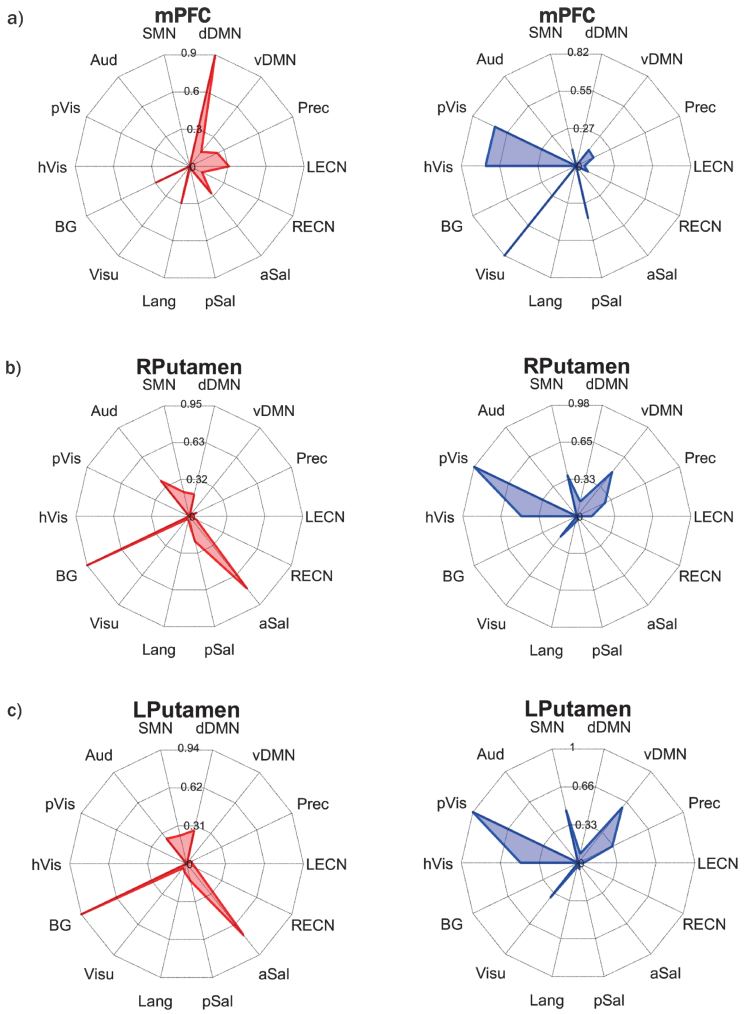

Fig. 4 FCOR spider plots for the three seed ROIs

Fig. 4a: mPFC
Fig. 4b: Right putamen
Fig. 4c: Left putamen

A FCOR analysis showed that positively correlated regions from the ROI in the mPFC had more than 90% overlap with the dorsal default mode network (Figure 4a). Five additional RSNs also significantly overlapped with the mPFC ROIs FC map, with FCOR values greater than 20%. Conversely, negatively correlated regions showed more than 80% overlap with the visuospatial network, more than 60% with primary and high visual networks, and more than 30% with the posterior salience network. As for basal ganglia (Figure 4b, c), seed ROIs in the putamen had FC maps that overlapped with more than 90% of the basal ganglia network and more than 60% of the anterior salience network. Significant but limited overlap regions also existed with the auditory, sensorimotor, and dorsal default mode networks. Negative FC maps overlapped with more than 90% of the primary visual network. Significant but limited overlap regions also existed in the ventral default mode, high visual, sensorimotor, precuneus, visuospatial and dorsal default mode networks.

a Sal: anterior salience network
Aud: auditory network
BG: basal ganglia network
dDMN: dorsal default mode network
FC: functional connectivity

FCOR: functional connectivity overlap ratio
hVis: high visual network
Lang: language network
LECN: left executive control network
mPFC: medial prefrontal cortex
Prec: precuneus network
pSal: posterior salience network
pVis: primary visual network
RECN: right executive control network
ROI: region of interest
RSNs: resting state networks
SMN: sensorimotor network
vDMN: ventral default mode network
Visu: visuospatial network

DISCUSSION

Spatial distribution of THK 5351 in normal aging

In this study, we identified an age-related spatial distribution of THK 5351 that tends to have higher concentrations in regions in the basal ganglia, medial prefrontal cortex, medial temporal lobe, hippocampus, thalamus, and orbitofrontal cortex in normal aging. Interestingly, the FC maps of the distribution's peaks in the medial prefrontal cortex and putamen strongly overlapped with the default mode and basal ganglia/salience networks. This suggests that the peak regions of the identified THK 5351 distribution pattern coincided with core regions of those networks. In addition, these peak regions were functionally connected to other several large-scale RSNs, implying their potential role in the between-network interaction known as the "connector hub".[32-35]

Association of THK 5351 with MAO-B

A recent study has shown that the topographical heterogeneity patterns of THK 5351 retention were consistent with the AD subtypes.[36] A postmortem study revealed that regional in vivo THK 5351 retention was significantly correlated with the density of tau aggregates associated with MAO-B, and glial fibrillary acidic protein in the neocortex, and MAO-B in the whole brain.[3] Taken together, THK 5351 retention in the AD neocortex would correspond to increased MAO-B/astrogliosis mainly associated with tau pathology in the human brain.

THK 5351 also showed retention in the brain of the patients with behavioral variant frontotemporal dementia[37,38] and nonfluent/agrammatic variant primary progressive aphasia[39] that corresponded to the clinical symptoms. In a case of Creutzfeldt-Jakob disease, THK 5351 uptake was increased in regions consistent with diffusion-restricted cortical areas on MRI and severe astrocytosis, which was reactive for MAO-B staining on postmortem study.[40] Rasagiline, a monoamine oxidase B inhibitor, reduces in vivo THK 5351 uptake in progressive supranuclear palsy.[41] These findings further support the view that THK 5351 will specifically bind to MAO-B.

The spatial distribution of age-related THK 5351 retention, as assessed by SSM/PCA, differed from age-related tau accumulation and spreading pattern except for the findings in the medial temporal lobe, basal forebrain, and olfactory areas.[42] However, the identified pattern was consistent with the regional prevalence of MAO-B in an autopsied human brain.[43] Although [18F]THK 5351 was initially developed as a tau-specific tracer, recent studies have shown that it also binds to MAO-B, which is mainly localized in the inner mitochondrial membrane of astrocytes and increases with astrogliosis.[2,3,44-46] Thus, we believe that THK 5351 mainly exhibited increasing MAO-B concentration in the brain with age in healthy subjects.

Relationship between distribution of THK 5351 and connector hubs of RSNs

Although it is well-known that MAO-B concentration related to astrogliosis in the brain will increase with age, this study is the first to elucidate its distribution patterns.

Interestingly, the peak locations of the primary THK5351 retention pattern coincide with core regions of the default mode and salience networks, which are two of the three known core neurocognitive networks (the third is the executive control network).[7] Several research findings have linked the aberrant functioning and organization of these networks to multiple psychiatric and neurological disorders, including AD, frontotemporal dementia, autism, and schizophrenia. In healthy aging, our recent study also showed that between-network connectivity among the core neurocognitive networks plus the basal ganglia network was associated with general cognitive performance.[47] This finding may suggest an important association of the role of these regions with general cognition and THK accumulation during aging.

Seed-based analysis from the peak region of THK 5351 in the mPFC showed strong positive connection to the default mode network and negative connection to the dorsal attention network. The default mode network, composed of the medial frontal gyrus, posterior cingulate cortex, bilateral angular gyrus, and hippocampus, is the most studied large-scale network. It is known to be deactivated during the execution of attention-demanding tasks. In contrast, the dorsal attention network is referred to as task-positive because it is generally activated during cognitive tasks requiring a response, such as visuospatial cueing tasks. The observed anticorrelation between these networks has been shown to exist.[48] This might be the point that distinguishes healthy aging from AD. Aside from these two networks, the peak region of THK 5351 in the mPFC was also connected with executive control, language, basal ganglia, precuneus, and anterior salience networks. Regions with diverse connections across other large-scale networks are called "connector hubs".[32-34] Connector hubs are important for the transfer of information among diverse networks of the brain.[35] Similarly, seed-based analysis from the peak region of THK 5351 in the bilateral putamen showed strongly positive connections to the basal ganglia network and salience network. Like the mPFC, these putaminal regions can be connector hubs, linking the anterior salience network and basal ganglia network. The salience network is believed to have a role in the identification of biologically and cognitively relevant events, to guide flexible behavior. The anterior insula and dorsal anterior cingulate cortex are major anchors of the salience network. The amygdala, the striatum, and the substantia nigra/ventral tegmental area are also crucial subcortical parts of the salience network and can provide access to the emotional and reward saliency of stimuli. Taken together, the peak regions of THK 5351 in the putamen may also serve as connector hubs and might communicate information concerning the basal ganglia network and anterior salience network, as well as the auditory, sensorimotor, and default mode networks.

As connector hubs, the above regions are characterized by continuous high baseline activity and/or associated metabolism. This may explain the preferential increasing MAO-B in these regions with aging. Hub regions are supposed to have excessive chronic neuronal activity associated with early neurodegeneration.[49]

Several studies have confirmed that THK 5351 accumulates on connector hubs in AD, particularly involving the precuneus/posterior cingulate cortex, dorsolateral prefrontal cortex, lateral parietal lobule (or involving all of the core neurocognitive networks, including executive control), but no study has been performed of healthy people. This study indicates that early MAO-B accumulation occurs in the connector hub regions of RSNs, which are supposed to require high energy in healthy subjects who show no accumulation of amyloid β, similar to AD. However, it is uncertain why THK 5351 accumulated on mPFC and putamen and not in other connector hubs. Further pathological and other PET studies, such as next-generation microglia ligands and pathological studies, will be required to clarify this idea and the continuity from healthy aging

to the development of neurodegenerative dementia.

DISCLOSURE STATEMENT

All authors declare that they have no conflicts of interest.

FUNDING

This work was supported by Grants-in-Aid from the Research Committee of Central Nervous System Degenerative Diseases by the Ministry of Health, Labour and Welfare, and from Integrated Research on Neuropsychiatric Disorders, project carried out under the Strategic Research for Brain Sciences by the Ministry of Education, Culture, Sports, Science and Technology of Japan. This work was also supported by a Grant-in-Aid for Scientific Research on Innovative Areas (Brain Protein Aging and Dementia Control; 26117002) from the Ministry of Education, Culture, Sports, Science and Technology (MEXT).

REFERENCES

1 Harada R, Okamura N, Furumoto S, et al. 18F-THK5351: A novel PET radiotracer for imaging neurofibrillary pathology in Alzheimer disease. *J Nucl Med*. 2016;57(2):208–214. doi:10.2967/jnumed.115.164848.
2 Ng KP, Pascoal TA, Mathotaarachchi S, et al. Monoamine oxidase B inhibitor, selegiline, reduces 18F-THK5351 uptake in the human brain. *Alzheimers Res Ther*. 2017;9(1):25. doi:10.1186/s13195-017-0253-y.
3 Harada R, Ishiki A, Kai H, et al. Correlations of 18F-THK5351 PET with postmortem burden of tau and astrogliosis in Alzheimer disease. *J Nucl Med*. 2018;59(4):671–674. doi:10.2967/jnumed.117.197426.
4 Tago T, Furumoto S, Okamura N, et al. Structure-activity relationship of 2-arylquinolines as PET imaging tracers for tau pathology in Alzheimer disease. *J Nucl Med*. 2016;57(4):608–614. doi:10.2967/jnumed.115.166652.
5 Ishibashi K, Kameyama M, Miura Y, Toyohara J, Ishii K. Head-to-Head Comparison of the Two MAO-B Radioligands, 18F-THK5351 and 11C-L-Deprenyl, to Visualize Astrogliosis in Patients with Neurological Disorders. *Clin Nucl Med*. 2021;46(1):e31-e33. doi:10.1097/RLU.0000000000003197.
6 Greicius M. Resting-state functional connectivity in neuropsychiatric disorders. *Curr Opin Neurol*. 2008;21(4):424–430. doi:10.1097/WCO.0b013e328306f2c5.
7 Menon V. Large-scale brain networks and psychopathology: A unifying triple network model. *Trends Cogn Sci*. 2011;15(10):483–506. doi:10.1016/j.tics.2011.08.003.
8 Dai Z, Yan C, Li K, et al. Identifying and mapping connectivity patterns of brain network hubs in Alzheimer's disease. *Cereb Cortex*. 2015;25(10):3723–3742. doi:10.1093/cercor/bhu246.
9 Greicius MD, Srivastava G, Reiss AL, Menon V. Default-mode network activity distinguishes Alzheimer's disease from healthy aging: Evidence from functional MRI. *Proc Natl Acad Sci U S A*. 2004;101(13):4637–4642. doi:10.1073/pnas.0308627101.
10 Hacker CD, Perlmutter JS, Criswell SR, Ances BM, Snyder AZ. Resting state functional connectivity of the striatum in Parkinson's disease. *Brain*. 2012;135(Pt 12):3699–3711. doi:10.1093/brain/aws281.
11 Kawabata K, Watanabe H, Hara K, et al. Distinct manifestation of cognitive deficits associate with different resting-state network disruptions in non-demented patients with Parkinson's disease. *J Neurol*. 2018;265(3):688–700. doi:10.1007/s00415-018-8755-5.
12 Yao N, Shek-Kwan Chang R, Cheung C, et al. The default mode network is disrupted in parkinson's disease with visual hallucinations. *Hum Brain Mapp*. 2014;35(11):5658–5666. doi:10.1002/hbm.22577.
13 Yokoi T, Watanabe H, Yamaguchi H, et al. Involvement of the precuneus/posterior cingulate cortex is significant for the development of Alzheimer's disease: A PET (THK5351, PiB) and resting fMRI study. *Front Aging Neurosci*. 2018;10:304. doi:10.3389/fnagi.2018.00304.
14 Yoneyama N, Watanabe H, Kawabata K, et al. Severe hyposmia and aberrant functional connectivity in cognitively normal Parkinson's disease. *PLoS One*. 2018;13(1):e0190072. doi:10.1371/journal.pone.0190072.

15 Song Z, Insel PS, Buckley S, et al. Brain amyloid-β burden is associated with disruption of intrinsic functional connectivity within the medial temporal lobe in cognitively normal elderly. *J Neurosci*. 2015;35(7):3240–3247. doi:10.1523/JNEUROSCI.2092-14.2015.
16 Lim HK, Nebes R, Snitz B, et al. Regional amyloid burden and intrinsic connectivity networks in cognitively normal elderly subjects. *Brain.* 2014;137(Pt 12):3327–3338. doi:10.1093/brain/awu271.
17 Moeller JR, Strother SC. A regional covariance approach to the analysis of functional patterns in positron emission tomographic data. *J Cereb Blood Flow Metab*. 1991;11(2):A121-A135. doi:10.1038/jcbfm.1991.47.
18 Alexander GE, Moeller JR. Application of the scaled subprofile model to functional imaging in neuropsychiatric disorders: A principal component approach to modeling brain function in disease. *Hum Brain Mapp*. 1994;2(1–2):79–94. doi:10.1002/hbm.460020108.
19 Spetsieris P, Ma Y, Peng S, et al. Identification of disease-related spatial covariance patterns using neuroimaging data. *J Vis Exp*. 2013;(76):50319. doi:10.3791/50319.
20 Shigemoto Y, Sone D, Ota M, et al. Voxel-based correlation of 18F-THK5351 accumulation and gray matter volume in the brain of cognitively normal older adults. *EJNMMI Res*. 2019;9(1):81. doi:10.1186/s13550-019-0552-3.
21 Mioshi E, Dawson K, Mitchell J, Arnold R, Hodges JR. The Addenbrooke's Cognitive Examination Revised (ACE-R): a brief cognitive test battery for dementia screening. *Int J Geriatr Psychiatry*. 2006;21(11):1078–1085. doi:10.1002/gps.1610.
22 Fazekas F, Kleinert R, Offenbacher H, et al. The morphologic correlate of incidental punctate white matter hyperintensities on MR images. *AJNR Am J Neuroradiol*. 1991;12(5):915–921.
23 Verdurand M, Bort G, Tadino V, Bonnefoi F, Le Bars D, Zimmer L. Automated radiosynthesis of the Pittsburg compound-B using a commercial synthesizer. *Nucl Med Commun*. 2008;29(10):920–926. doi:10.1097/MNM.0b013e328304e0e1.
24 Hammers A, Allom R, Koepp MJ, et al. Three-dimensional maximum probability atlas of the human brain, with particular reference to the temporal lobe. *Hum Brain Mapp*. 2003;19(4):224–247. doi:10.1002/hbm.10123.
25 Jack CR Jr, Lowe VJ, Weigand SD, et al. Serial PIB and MRI in normal, mild cognitive impairment and Alzheimers disease: implications for sequence of pathological events in Alzheimers disease. *Brain*. 2009;132(Pt 5):1355–1365. doi:10.1093/brain/awp062.
26 Bourgeat P, Chételat G, Villemagne VL, et al. Beta-amyloid burden in the temporal neocortex is related to hippocampal atrophy in elderly subjects without dementia. *Neurology*. 2010;74(2):121–127. doi:10.1212/WNL.0b013e3181c918b5.
27 Villemagne VL, Pike KE, Chételat G, et al. Longitudinal assessment of Aβ and cognition in aging and Alzheimer disease. *Ann Neurol*. 2011;69(1):181–192. doi:10.1002/ana.22248.
28 Villemagne VL, Burnham S, Bourgeat P, et al. Amyloid β deposition, neurodegeneration, and cognitive decline in sporadic Alzheimer's disease: a prospective cohort study. *Lancet Neurol*. 2013;12(4):357–367. doi:10.1016/S1474-4422(13)70044-9.
29 Niethammer M, Tang CC, Feigin A, et al. A disease-specific metabolic brain network associated with corticobasal degeneration. *Brain*. 2014;137(Pt 11):3036–3046. doi:10.1093/brain/awu256.
30 Shirer WR, Ryali S, Rykhlevskaia E, Menon V, Greicius MD. Decoding subject-driven cognitive states with whole-brain connectivity patterns. *Cereb Cortex*. 2012;22(1):158–165. doi:10.1093/cercor/bhr099.
31 Bagarinao E, Watanabe H, Maesawa S, et al. Identifying the brain's connector hubs at the voxel level using functional connectivity overlap ratio. *Neuroimage*. 2020;222:117241. doi:10.1016/j.neuroimage.2020.117241.
32 van den Heuvel MP, Sporns O. Network hubs in the human brain. *Trends Cogn Sci*. 2013;17(12):683–696. doi:10.1016/j.tics.2013.09.012.
33 Bertolero MA, Yeo BTT, D'Esposito M. The modular and integrative functional architecture of the human brain. *Proc Natl Acad Sci U S A*. 2015;112(49):E6798-E6807. doi:10.1073/pnas.1510619112.
34 Bertolero MA, Yeo BTT, D'Esposito M. The diverse club. *Nat Commun*. 2017;8(1):1277. doi:10.1038/s41467-017-01189-w.
35 Bertolero MA, Yeo BTT, Bassett DS, D'Esposito M. A mechanistic model of connector hubs, modularity and cognition. *Nat Hum Behav*. 2018;2(10):765–777. doi:10.1038/s41562-018-0420-6.
36 Jeon S, Kang JM, Seo S, et al. Topographical Heterogeneity of Alzheimer's Disease Based on MR Imaging, Tau PET, and Amyloid PET. *Front Aging Neurosci*. 2019;11:211. doi:10.3389/fnagi.2019.00211.
37 Nam G, Jeong HJ, Kang JM, et al. ^{18}F-THK5351 PET Imaging in the Behavioral Variant of Frontotemporal Dementia. *Dement Neurocogn Disord*. 2018;17(4):163–173. doi:10.12779/dnd.2018.17.4.163.
38 Son HJ, Oh JS, Roh JH, et al. Differences in gray and white matter ^{18}F-THK5351 uptake between behavioral-variant frontotemporal dementia and other dementias. *Eur J Nucl Med Mol Imaging*. 2019;46(2):357–366.

doi:10.1007/s00259-018-4125-x.
39 Yoon CW, Jeong HJ, Seo S, et al. ^{18}F-THK5351 PET Imaging in Nonfluent-Agrammatic Variant Primary Progressive Aphasia. *Dement Neurocogn Disord*. 2018;17(3):110–119. doi:10.12779/dnd.2018.17.3.110.
40 Kim HJ, Cho H, Park S, et al. THK5351 and flortaucipir PET with pathological correlation in a Creutzfeldt-Jakob disease patient: a case report. *BMC Neurol*. 2019;19(1):211. doi:10.1186/s12883-019-1434-z.
41 Ng KP, Therriault J, Kang MS, et al. Rasagiline, a monoamine oxidase B inhibitor, reduces in vivo [^{18}F] THK5351 uptake in progressive supranuclear palsy. *Neuroimage Clin*. 2019;24:102091. doi:10.1016/j.nicl.2019.102091.
42 Crary JF, Trojanowski JQ, Schneider JA, et al. Primary age-related tauopathy (PART): a common pathology associated with human aging. *Acta Neuropathol*. 2014;128(6):755–766. doi:10.1007/s00401-014-1349-0.
43 Tong J, Meyer JH, Furukawa Y, et al. Distribution of monoamine oxidase proteins in human brain: Implications for brain imaging studies. *J Cereb Blood Flow Metab*. 2013;33(6):863–871. doi:10.1038/jcbfm.2013.19.
44 Levitt P, Pintart JE, Breakefieldt XO. Immunocytochemical demonstration of monoamine oxidase B in brain astrocytes and serotonergic neurons. *Proc Natl Acad Sci U S A*. 1982;79(20):6385–6389. doi:10.1073/pnas.79.20.6385.
45 Ekblom J, Jossan SS, Bergström M, Oreland L, Walum E, Aquilonius SM. Monoamine oxidase-B in astrocytes. *Glia*. 1993;8(2):122–132. doi:10.1002/glia.440080208.
46 Lemoine L, Gillberg PG, Svedberg M, et al. Comparative binding properties of the tau PET tracers THK5117, THK5351, PBB3, and T807 in postmortem Alzheimer brains. *Alzheimers Res Ther*. 2017;9(1):96. doi:10.1186/s13195-017-0325-z.
47 Bagarinao E, Watanabe H, Maesawa S, et al. Reorganization of brain networks and its association with general cognitive performance over the adult lifespan. *Sci Rep*. 2019;9(1):11352. doi:10.1038/s41598-019-47922-x.
48 Uddin LQ, Kelly AM, Biswal BB, Castellanos FX, Milham MP. Functional connectivity of default mode network components: correlation, anticorrelation, and causality. *Hum Brain Mapp*. 2009;30(2):625–637. doi:10.1002/hbm.20531.
49 de Haan W, Mott K, van Straaten EC, Scheltens P, Stam CJ. Activity dependent degeneration explains hub vulnerability in Alzheimer's disease. *PLoS Comput Biol*. 2012;8(8):e1002582. doi:10.1371/journal.pcbi.1002582.